

A Splitting-free Vorticity Redistribution Method

M. Kirchhart¹, S. Obi

*Department of Mechanical Engineering, Keio University, 3-14-1 Hiyoshi, Kōhoku-ku,
Yokohama-shi 233-8522, Japan*

Abstract

We present a splitting-free variant of the vorticity redistribution method. Spatial consistency and stability when combined with a time-stepping scheme are proven. We propose a new strategy preventing excessive growth in the number of particles while retaining the order of consistency. The novel concept of small neighbourhoods significantly reduces the method's computational cost. In numerical experiments the method showed second order convergence, one order higher than predicted by the analysis. Compared to the fast multipole code used in the velocity computation, the method is about three times faster.

Keywords: Vortex Diffusion Schemes, Vortex Particle Methods

1. Introduction

In vortex methods in two dimensions and in the absence of boundaries, one wants to evolve a scalar vorticity field ω in form of a *particle cloud*:

$$\omega(t, \mathbf{x}) = \sum_{i=1}^N \Gamma_i(t) \delta(\mathbf{x} - \mathbf{x}_i(t)), \quad (1)$$

over time t according to the vorticity transport equation:

$$\frac{D\omega}{Dt} \equiv \frac{\partial\omega}{\partial t} + (\mathbf{u} \cdot \nabla)\omega = \nu\Delta\omega. \quad (2)$$

In there, $\Gamma_i \in \mathbb{R}$ denotes the circulation that particle i carries, $\mathbf{x}_i \in \mathbb{R}^2$ stands for that particle's position, $\mathbf{u} : \mathbb{R}^2 \rightarrow \mathbb{R}^2$ is the velocity field induced by ω according

Email addresses: kirchhart@keio.jp (M. Kirchhart), obsn@mech.keio.ac.jp (S. Obi)

¹Corresponding author

to the Biot–Savart law, $\nu \geq 0$ refers to the fluid’s kinematic viscosity, and δ is the Dirac delta distribution.

The beauty of vortex methods lies in their handling of the inviscid case ($\nu = 0$): evolving Γ_i and \mathbf{x}_i according to the following set of ordinary differential equations (ODEs):

$$\begin{aligned} \frac{d\mathbf{x}_i}{dt} &= \mathbf{u}(t, \mathbf{x}_i(t)), \\ \frac{d\Gamma_i}{dt} &= 0, \end{aligned} \tag{3}$$

i. e., by convecting the particles according to the local velocity and leaving their strengths unchanged, the resulting vorticity field fulfils the vorticity transport equation (2) exactly. Especially, due to the absence of a fixed computational mesh and the natural treatment of convection, inviscid vortex methods are *free of numerical dissipation* and conserve circulation, linear and angular momentum, as well as energy exactly [1].

Many different approaches on how to handle the viscous case have been suggested in the literature, the book by Cottet and Koumoutsakos [1] gives an overview and references to some of the most commonly used approaches. Almost all of them belong to the class of *viscous-splitting* algorithms: first, particles are convected under the absence of viscosity. Afterwards vorticity is diffused according to the heat-equation, i. e., in absence of convection. One of the earliest such approaches is the so-called ‘random-walk’ method, in which viscosity is simulated by an additional Brownian motion of the particles. This method, however, converges only very slowly.

The resurrected core-spreading technique [2] relies on a different representation of the vorticity field (1). The Biot–Savart kernel is singular at the origin, causing very large velocity values when particles approach each other. For this reason the Biot–Savart law is usually regularised in practice. This is commonly done by replacing the Dirac delta distribution δ with a smooth approximation ζ_ε , a so-called blob-function with blob- or core-width ε . As the name suggests, the core-spreading method works by enlarging individual particle’s core

widths ε . This enlargement causes the solution to get increasingly blurred over time, unless some kind of remeshing is employed.

The method of particle strength exchange (PSE), on the other hand, modifies the particle strengths by approximating the Laplacian by an integral. This integral is then approximated by numerical quadrature, using the particle positions as quadrature nodes. Frequent remeshing is required, unless the newer mesh-free variant DC-PSE [3] is employed.

The vorticity redistribution method (VRM) by Shankar and van Dommelen [4] can be interpreted as a computed finite-difference stencil which solves the heat-equation for a given time-step Δt . The fact that these stencils are computed on-the-fly makes the method completely mesh-free.

While most of these methods achieve high-order spatial accuracy, the viscous-splitting inevitably limits their accuracy in time to first order, unless more sophisticated splits are used [5]. Note that this result holds regardless of the time-stepping scheme used, underlining that splitting the equation is unnatural: diffusion and convection *do happen simultaneously* and thus should not be treated one after another.

Our contribution in this article is a new method of treating the diffusive term in a manner similar to the vorticity redistribution method (VRM). Instead of computing a stencil that approximates a solution to the heat equation, we directly approximate the Laplacian. This allows us to avoid the viscous-splitting and to treat both diffusion and convection simultaneously. The spatial consistency of our method is proven. As we do not need to integrate the Laplacian over time, our proof does not require Fourier analysis, like the original VRM. We then consider the case of pure diffusion in combination with the forward Euler method and derive sharp a-priori and a-posteriori bounds on the step-width. This analysis in the absence of convection is justified, as the convective part of the equations is known to be stable independent of the step-width [6]. The resulting a-priori bound is—apart from a constant—identical to the classical stability condition for the five-point central-difference stencil, underlining the interpretation of our method as a computed finite-difference method.

Finally, we show that our method conserves circulation, linear, and angular momentum. In the original VRM-paper it was suggested to ignore particles in the diffusive process if their circulation was below a certain threshold. Choosing a low threshold does yield accurate discretisations, however, the choice of its value seemed rather arbitrary. We propose a new strategy preventing excessive growth in the number of particles while maintaining the order of consistency. Based on results by Seibold [7, 8], we further introduce the new concept of *small neighbourhoods* which significantly reduces the computational cost of the method. The resulting scheme keeps all of the benefits of the original VRM while not relying on viscous splitting or arbitrary thresholds. We conclude with numerical examples illustrating efficiency and convergence of the method in the purely diffusive, as well as in the convective case.

2. Description of the Method

Our aim is to approximate the Laplacian of ω by the following formula:

$$\Delta_h \omega := \sum_{i=1}^N \sum_{j=1}^N f_{ij} \Gamma_i \delta(\mathbf{x} - \mathbf{x}_j), \quad (4)$$

where $f_{ij} \Gamma_i$ refers to the rate at which circulation is diffused from particle i to particle j . The values of f_{ij} need to be chosen such that certain conditions are fulfilled in order for this approximation to be accurate.

In order to specify these conditions, we assume that the particles are quasi-uniformly distributed, with h corresponding to the average inter-particle spacing. We then define the neighbourhood \mathcal{N}_i of particle i as follows:

$$\mathcal{N}_i := \{j \in 1, \dots, N : rh \leq |\mathbf{x}_i - \mathbf{x}_j| \leq Rh\} \cup \{i\}. \quad (5)$$

where $R > r > 0$ are fixed, user-defined parameters. The original VRM formulation does not include the lower bound r . Due to their movement, particles might get closer to one another than this. In section 6.2 we will give some remarks on this problem. In our analysis we show that both bounds are required to control the error: the upper bound limits the cut-off error of the expansions

used, while the lower bound is needed for stability. For $j \in \mathcal{N}_i$ the values f_{ij} are chosen such that certain moment conditions are fulfilled. For $j \notin \mathcal{N}_i$ we define $f_{ij} = 0$.

As will be seen later on, depending on the particle cloud's geometry, these moment conditions do not always have a solution. Note, however, that we can always add new particles of zero strength to the field: introducing a new particle with $\Gamma_i = 0$ leaves the vorticity field (1) unchanged. In this point the VRM slightly differs from classical finite-difference methods: the vorticity field (1) is not a list of pointwise function values; rather it can be seen as a quadrature rule for integrating functions against an underlying, smooth vorticity field. Inserting an empty particle corresponds to adding a quadrature node with weight zero.

For such empty particles one obviously always has $\Gamma_i = 0 \implies f_{ij}\Gamma_i = 0$, i. e., the value of f_{ij} is arbitrary and can safely be defined as zero, too. We make use of this fact by inserting new particles to fill holes in the cloud and to expand it at its outer rim. This way we can ensure that for all circulation-carrying particles sufficiently many neighbours do exist. Circulation will then be diffused to the neighbouring particles and thereby be spread out in space, which also is in accordance with the physical intuition of diffusive processes.

At the core of our method lies the computation of the values f_{ij} for every i and $j \in \mathcal{N}_i$. In order to ensure accuracy, the error is developed as a Taylor expansion. We require that at least all error terms of constant, linear, and quadratic order vanish. For second order accuracy one may also choose to require cubic terms to vanish. A detailed derivation of the resulting equations is given in section 3.2.

As will be seen later on, non-negativity of stencils is a sufficient criterion for stable time-discretisations. In addition to that, such stencils possess many more desirable properties, as described by Seibold [7, 8, 9]. A stencil is called non-negative if it fulfils $f_{ij} \geq 0$ for all $j \neq i$. Unfortunately, as also will be shown in the analysis section 3.6, non-negative stencils cannot fulfil the moment equations of fourth order. Unless one gives up on non-negativity and the resulting stability guarantee, the method's accuracy is hence limited to second order.

Like the two-dimensional Taylor expansion, the moment conditions are most easily expressed using multi-index notation. Defining the vector \mathbf{r}_{ij} :

$$\mathbf{r}_{ij} = \mathbf{x}_j - \mathbf{x}_i, \quad (6)$$

and denoting its Cartesian components by \mathbf{r}_{ij}^x and \mathbf{r}_{ij}^y , respectively, for $\mathcal{O}(h^n)$ accuracy, with $n = 1$ or $n = 2$, we pose the following conditions:

$$\sum_{j=1}^N f_{ij} \mathbf{r}_{ij}^x \mathbf{r}_{ij}^x = 2, \quad \sum_{j=1}^N f_{ij} \mathbf{r}_{ij}^y \mathbf{r}_{ij}^y = 2, \quad \sum_{j=1}^N f_{ij} \mathbf{r}_{ij}^x \mathbf{r}_{ij}^y = 0, \quad (7)$$

and for all other error terms with multi-index α :

$$\sum_{j=1}^N f_{ij} \mathbf{r}_{ij}^\alpha = 0, \quad 0 \leq |\alpha| \leq n + 1, \quad |\alpha| \neq 2. \quad (8)$$

Because we have $\mathbf{r}_{ii} \equiv \mathbf{0}$, only the equation for $\alpha = (0, 0)$ depends on f_{ii} , yielding:

$$f_{ii} = - \sum_{j \neq i} f_{ij}. \quad (9)$$

For $n = 1, 2$ we consequently have to solve a system consisting of five or nine moment conditions, respectively. For every particle i , this linear system can be rewritten in matrix-vector notation:

$$\mathbf{V}_i \mathbf{f}_i = \mathbf{b}, \quad \mathbf{f}_i \geq 0. \quad (10)$$

Here, \mathbf{f}_i is the vector of coefficients f_{ij} , $i \neq j$, \mathbf{b} is the vector that contains only zero entries except for the two ‘2’-entries at $\alpha = (2, 0)$ and $\alpha = (0, 2)$, and \mathbf{V}_i is the Vandermonde-matrix, with rows for each multi-index $1 \leq |\alpha| \leq n + 1$ and columns j for each particle $j \in \mathcal{N}_i \setminus \{i\}$:

$$V_{\alpha,j} = \mathbf{r}_{ij}^\alpha. \quad (11)$$

In order to obtain scaling independent of h , for a numerical implementation it is beneficial and straightforward to rewrite these conditions for the normalised vectors \mathbf{r}_{ij}/h . In section 4 we describe how to solve these equations and how to ensure that non-negative stencils exist.

3. Analysis

3.1. Preliminaries

Let $n \in \{1, 2\}$ be the desired order of accuracy, let $p \in [1, \infty)$ be arbitrary but fixed, let q be its conjugate exponent such that $1 = 1/p + 1/q$, and let k be an integer such that $k > 2/p + n + 2$. We denote the Sobolev space of k times weakly differentiable $L^p(\mathbb{R}^2)$ -functions by $W^{k,p}$, and let $W^{-k,q}$ refer to its dual space. Note that, by the Sobolev embedding theorem, we have $W^{k,p} \hookrightarrow C^{n+2}$, where C^{n+2} refers to the space of $n + 2$ times continuously differentiable functions equipped with the maximum norm over all derivatives. Further note that we have $\|(\Gamma_i)\|_{l^1} < \infty$, and therefore $\omega(t, \cdot) \in W^{-k,q}$:

$$\begin{aligned} \|\omega\|_{W^{-k,q}} &= \sup_{\varphi \in W^{k,p}} \frac{\langle \omega, \varphi \rangle}{\|\varphi\|_{W^{k,p}}} \leq \sup_{\varphi \in W^{k,p}} C_{\text{emb}} \frac{\sum_{i=1}^N |\Gamma_i| |\varphi(\mathbf{x}_i)|}{\|\varphi\|_{C^{n+2}}} \\ &\leq \sup_{\varphi \in W^{k,p}} C_{\text{emb}} \frac{\|\varphi\|_{C^{n+2}} \sum_{i=1}^N |\Gamma_i|}{\|\varphi\|_{C^{n+2}}} = C_{\text{emb}} \|(\Gamma_i)\|_{l^1}, \end{aligned} \quad (12)$$

where $\langle \cdot, \cdot \rangle$ refers to the dual pairing and C_{emb} denotes the Sobolev embedding constant. This inequality also allows us to infer stability in the $\|\cdot\|_{W^{-k,q}}$ -norm by bounding the l^1 -norm of the circulations later on.

3.2. Consistency

We will need the following lemma.

Lemma 1. *For a stencil that satisfies (10) one has:*

$$f_{ii} = - \sum_{j \neq i} f_{ij} \leq 0, \quad 4(Rh)^{-2} \leq \sum_{j \neq i} f_{ij} \leq 4(rh)^{-2}. \quad (13)$$

PROOF. The first part directly follows from $f_{ij} \geq 0$ for $i \neq j$ and equation (9). The second relation follows by the sum of the moment equations for $\alpha = (2, 0)$ and $\alpha = (0, 2)$ and $rh \leq |\mathbf{r}_{ij}| \leq Rh$. \square

We now are ready to prove the following consistency result.

Theorem 1 (Consistency). *One has:*

$$\|\Delta\omega - \Delta_h\omega\|_{W^{-k,q}} \leq C \left(\frac{R}{r}\right)^2 (Rh)^n \|(\Gamma_i)\|_{l^1},$$

where C is a constant that only depends on n .

PROOF. For arbitrary $\varphi \in W^{k,p}$ one has:

$$\langle \Delta\omega - \Delta_h\omega, \varphi \rangle = \sum_{i=1}^N \Gamma_i \left(\Delta\varphi(\mathbf{x}_i) - \sum_{j=1}^N f_{ij}\varphi(\mathbf{x}_j) \right). \quad (14)$$

We develop $\varphi(\mathbf{x}_j)$ as a Taylor series around $\varphi(\mathbf{x}_i)$ and obtain:

$$\varphi(\mathbf{x}_j) = \sum_{|\alpha| \leq n+1} \frac{\mathbf{r}_{ij}^\alpha}{\alpha!} D^\alpha \varphi(\mathbf{x}_i) + \underbrace{\sum_{|\alpha|=n+2} \frac{\mathbf{r}_{ij}^\alpha}{\alpha!} D^\alpha \varphi(\boldsymbol{\xi}_{ij})}_{=: R_{ij}^{n+2}}, \quad (15)$$

where $\boldsymbol{\xi}_{ij}$ is a point on the line connecting \mathbf{x}_i and \mathbf{x}_j . The moment conditions were chosen such that the first sum vanishes when this relation is inserted into equation (14). Note that we have with the help of the Sobolev embedding:

$$|R_{ij}^{n+2}| \leq C_{\text{emb}} C_\alpha (Rh)^{n+2} \|\varphi\|_{W^{k,p}}, \quad C_\alpha = \sum_{|\alpha|=n+2} \frac{1}{\alpha!}, \quad (16)$$

such that we get with the help of the triangle inequality, Hölder's inequality, and Lemma 1:

$$\begin{aligned} |\langle \Delta\omega - \Delta_h\omega, \varphi \rangle| &= \left| \sum_{i=1}^N \Gamma_i \sum_{j=1}^N f_{ij} R_{ij}^{n+2} \right| \leq \|(\Gamma_i)\|_{l^1} \left\| \left(\sum_{j=1}^N f_{ij} R_{ij}^{n+2} \right)_i \right\|_{l^\infty} \\ &\leq 4C_{\text{emb}} C_\alpha \frac{(Rh)^{n+2}}{(rh)^2} \|\varphi\|_{W^{k,p}} \|(\Gamma_i)\|_{l^1}. \end{aligned} \quad (17)$$

□

3.3. Stability for the Heat Equation

In our next step we investigate the stability of Euler's method in combination with our spatial discretisation. As we introduced a new discretisation of the Laplace operator, it is natural to omit convection and to investigate the heat equation:

$$\frac{\partial \omega}{\partial t} = \nu \Delta \omega. \quad (18)$$

We are going to apply the method of lines: in our case ω is a particle cloud, the Laplacian operator is replaced with its discretisation Δ_h , and the time derivative is discretised using Euler's method. While this method is only first-order accurate, this all that is needed to construct higher order schemes: so-called non-linear SSP-stable methods of higher order exist, which can be written

as a convex combination of several Euler steps [10]. While the classical Runge–Kutta method (RK4) is not such a scheme, our numerical experiments exhibited no instabilities.

To ease notation, we introduce the vector $\Gamma \in \mathbb{R}^N$, consisting of the components Γ_i , and the matrix $F \in \mathbb{R}^{N \times N}$, consisting of components f_{ij} , respectively. Denoting the current and next time-steps with n and $n + 1$, respectively, our scheme then reads:

$$\Gamma^{n+1} = \underbrace{(I + \nu \Delta t F^\top)}_{=:C} \Gamma^n, \quad (19)$$

where $I \in \mathbb{R}^{N \times N}$ is the identity matrix and $\Delta t > 0$ denotes the step-width. As shown in theorem 1, the consistency error can be bounded by $\|\Gamma\|_1$. It is therefore sufficient to require $\|C\|_1 \leq 1$. Note that due to equation (12), this implies that $\|\omega\|_{W^{-k,q}}$ remains bounded as well. The following theorem will show that positive stencils are not only sufficient but also necessary to obtain a scheme that fulfils $\|C\|_1 \leq 1$.

Theorem 2 (Stability). *One has:*

$$\|C\|_1 = 1,$$

if and only if we have a positive stencil:

$$f_{ii} \leq 0, \quad f_{ij} \geq 0 \quad (i \neq j)$$

and for all $i = 1, \dots, N$:

$$\nu \Delta t \leq -f_{ii}^{-1}.$$

For larger Δt or non-positive stencils one always has $\|C\|_1 > 1$.

PROOF. One has:

$$\|C\|_1 = \max_j \sum_{i=1}^N |C_{ij}| = \max_j |1 + \nu \Delta t f_{jj}| + \nu \Delta t \sum_{i \neq j} |f_{ji}|. \quad (20)$$

Thus $\|C\|_1 \leq 1 \implies f_{jj} \leq 0$. Now assume $(1 + \nu \Delta t f_{jj}) \geq 0$, i. e., $\nu \Delta t \leq -f_{jj}^{-1}$.

We then have for each j , due to equation (9):

$$\sum_{i=1}^N |C_{ij}| = 1 - \nu \Delta t \sum_{i \neq j} f_{ji} + \nu \Delta t \sum_{i \neq j} |f_{ji}|. \quad (21)$$

Thus, we have $\|\mathbf{C}\|_1 \leq 1$ if and only if for all j :

$$\sum_{i \neq j} |f_{ji}| \leq \sum_{i \neq j} f_{ji} \iff f_{ji} \geq 0. \quad (22)$$

For positive stencils both sides are equal, and thus $\|\mathbf{C}\|_1 = 1$.

Conversely assume $(1 + \nu\Delta t f_{jj}) < 0$, i. e., $\nu\Delta t > -f_{jj}^{-1}$. We then have again due to equation (9):

$$\sum_{i=1}^N |C_{ij}| = -1 + \nu\Delta t \sum_{i \neq j} (f_{ij} + |f_{ij}|). \quad (23)$$

Assume we would have $\|\mathbf{C}\|_1 \leq 1$. We then would have for all j :

$$\sum_{i \neq j} (f_{ij} + |f_{ij}|) \leq \frac{2}{\nu\Delta t}. \quad (24)$$

But note that we have:

$$\sum_{i \neq j} (f_{ij} + |f_{ij}|) \geq 2 \sum_{i \neq j} f_{ij} = 2f_{jj}, \quad (25)$$

and thus:

$$2f_{jj} \leq \frac{2}{\nu\Delta t} \iff \nu\Delta t \leq -f_{jj}^{-1}, \quad (26)$$

which is a direct contradiction to our assumption on the time-step. \square

Theorem 2 gives us an easy a-posteriori bound which can readily be implemented. This allows us to optimally choose the step-width in a computer program. In higher-order Runge–Kutta schemes it is hard to predict the values f_{ii} for intermediate stages. Thus, again employing Lemma 1, the following a-priori bound is useful:

$$\Delta t \leq \frac{(rh)^2}{4\nu}. \quad (27)$$

Note that this closely resembles the classical stability condition for the five-point finite-difference stencil, highlighting the similarity between the two methods. The fact that we can only achieve $\|\mathbf{C}\|_1 = 1$, as opposed to $\|\mathbf{C}\|_1 < 1$, can be seen as a consequence of the fact that our method conserves circulation, as will be shown in the next section.

3.4. Conservation Properties for the Navier–Stokes Equations

We now discuss the conservation properties of our method when used in combination with convection, i. e., for the Navier–Stokes equations. We thus consider the following semi-discrete system of coupled ordinary differential equations:

$$\begin{aligned}\frac{d\mathbf{x}_i}{dt} &= \sum_{j=1}^N \mathbf{K}(\mathbf{r}_{ij})\Gamma_j, \\ \frac{d\Gamma_i}{dt} &= \nu \sum_{j=1}^N f_{ji}\Gamma_j,\end{aligned}\tag{28}$$

where \mathbf{K} denotes the Biot–Savart kernel defined for $\mathbf{x} = (x, y) \in \mathbb{R}^2$ as:

$$\mathbf{K}(\mathbf{x}) := \begin{cases} \mathbf{0} & \text{if } \mathbf{x} = \mathbf{0}, \\ \frac{(y, -x)^\top}{2\pi|\mathbf{x}|^2} & \text{else.} \end{cases}\tag{29}$$

Note that we differ from the usual sign convention, such that we do not need to negate the vector \mathbf{r}_{ij} in equation (28). Also note that the fractions f_{ij} depend on the particle positions, which we, for reasons of brevity, did not introduce into the notation. We are going to investigate the following quantities:

- Circulation: $I_0 := \int_{\mathbb{R}^2} \omega \, d\mathbf{x} = \sum_{i=0}^N \Gamma_i$,
- Linear Momentum: $\mathbf{I}_1 := \int_{\mathbb{R}^2} \omega \mathbf{x} \, d\mathbf{x} = \sum_{i=0}^N \Gamma_i \mathbf{x}_i$,
- Angular Momentum: $I_2 := \int_{\mathbb{R}^2} \omega \mathbf{x}^2 \, d\mathbf{x} = \sum_{i=0}^N \Gamma_i \mathbf{x}_i^2$.

The conservation laws for these quantities read [11, 12]:

$$\frac{dI_0}{dt} = 0, \quad \frac{d\mathbf{I}_1}{dt} = \mathbf{0}, \quad \frac{dI_2}{dt} = 4\nu I_0.\tag{30}$$

Note that these quantities are moments of vorticity and thus are closely linked to the moment conditions (8) and (7). This close link will allow us to show that the semi-discrete equations (28) fulfil the conservation laws (30) exactly.

Theorem 3 (Conservation of Circulation and Momentum). *The vorticity field described by the system of ODEs (28) conserves circulation as well as linear and angular momentum.*

PROOF. Our proof utilises the moment conditions as well as ideas from Cottet and Koumoutsakos [1]. For circulation we immediately obtain:

$$\frac{dI_0}{dt} = \sum_{i=1}^N \frac{d\Gamma_i}{dt} = \nu \sum_{i=1}^N \sum_{j=1}^N f_{ji} \Gamma_j = \nu \sum_{j=1}^N \Gamma_j \underbrace{\sum_{i=1}^N f_{ji}}_{=0} = 0. \quad (31)$$

For linear momentum we have:

$$\frac{d\mathbf{I}_1}{dt} = \sum_{i=1}^N \Gamma_i \frac{d\mathbf{x}_i}{dt} + \sum_{i=1}^N \mathbf{x}_i \frac{d\Gamma_i}{dt}. \quad (32)$$

For the first part of the sum note that the Biot–Savart kernel is odd, i. e., we have $\mathbf{K}(\mathbf{r}_{ij}) = -\mathbf{K}(\mathbf{r}_{ji})$. Using this relation and exchanging the indices we obtain:

$$\sum_{i=1}^N \Gamma_i \frac{d\mathbf{x}_i}{dt} = \sum_{i=1}^N \sum_{j=1}^N \mathbf{K}(\mathbf{r}_{ij}) \Gamma_i \Gamma_j = - \sum_{i=1}^N \sum_{j=1}^N \mathbf{K}(\mathbf{r}_{ij}) \Gamma_i \Gamma_j. \quad (33)$$

Thus, this part of the sum equals its negative and therefore is zero. For the second part we have using the moment conditions:

$$\nu \sum_{i=1}^N \sum_{j=1}^N f_{ji} \Gamma_j \mathbf{x}_i = \nu \sum_{j=1}^N \Gamma_j \left(\underbrace{\sum_{i=1}^N f_{ji} \mathbf{r}_{ji}}_{=0} + \mathbf{x}_j \underbrace{\sum_{i=1}^N f_{ji}}_{=0} \right) = \mathbf{0}. \quad (34)$$

Lastly, for the angular momentum we obtain:

$$\frac{dI_2}{dt} = \sum_{i=1}^N 2\Gamma_i \mathbf{x}_i \cdot \frac{d\mathbf{x}_i}{dt} + \sum_{i=1}^N \mathbf{x}_i^2 \frac{d\Gamma_i}{dt}. \quad (35)$$

For the first sum we have:

$$2 \sum_{i=1}^N \sum_{j=1}^N \Gamma_i \Gamma_j \mathbf{K}(\mathbf{r}_{ij}) \cdot \mathbf{x}_i. \quad (36)$$

By writing $\mathbf{x}_i = 1/2(\mathbf{x}_i + \mathbf{x}_j) + 1/2(\mathbf{x}_i - \mathbf{x}_j)$ this sum again splits up into two parts. Using the oddness property of \mathbf{K} and exchanging the indices as above,

the first part is zero. For the second part note that by the definition of \mathbf{K} we have $\mathbf{K}(\mathbf{r}_{ij}) \cdot \mathbf{r}_{ij} \equiv 0$. Finally, we have $\mathbf{x}_i^2 = \mathbf{r}_{ji}^2 + 2\mathbf{x}_i^x \mathbf{x}_j^x + 2\mathbf{x}_i^y \mathbf{x}_j^y - \mathbf{x}_j^2$ and thus:

$$\begin{aligned} \sum_{i=1}^N \mathbf{x}_i^2 \frac{d\Gamma_i}{dt} &= \nu \sum_{i=1}^N \sum_{j=1}^N f_{ji} \Gamma_j \mathbf{x}_i^2 = \\ &= \nu \sum_{j=1}^N \Gamma_j \left(\underbrace{\sum_{i=1}^N f_{ji} \mathbf{r}_{ji}^2}_{=4} + 2\mathbf{x}_j^x \underbrace{\sum_{i=1}^N f_{ji} \mathbf{x}_i^x}_{=0} + 2\mathbf{x}_j^y \underbrace{\sum_{i=1}^N f_{ji} \mathbf{x}_i^y}_{=0} - \mathbf{x}_j^2 \underbrace{\sum_{i=1}^N f_{ji}}_{=0} \right) = \\ &= 4\nu \sum_{i=1}^N \Gamma_i = 4\nu I_0. \end{aligned} \quad (37)$$

□

Due to the non-linear coupling of Γ_i and \mathbf{x}_i in \mathbf{I}_1 and \mathbf{I}_2 , these quantities are generally not exactly conserved when the system of ODEs (28) is discretised using Euler's method. Here, one can only verify I_0 to be conserved exactly. The numerical experiments at the end of this article have shown, however, that the other two quantities are conserved very well in practice.

At the end we want to remark that kinetic energy E :

$$E = \int_{\mathbb{R}^2} \omega(y\mathbf{u}^x - x\mathbf{u}^y) d\mathbf{x} \quad (38)$$

contains a product with the velocity \mathbf{u} , which is non-linearly linked to ω and the particle positions through the Biot–Savart law. As the moment conditions do not reflect this, we cannot expect the scheme to conserve energy exactly.

3.5. Reducing the Number of Diffused Particles

When used as introduced above, the method may give rise to large numbers of particles carrying negligible amount of circulation, thus unnecessarily increasing the numerical cost. For this reason, Shankar and van Dommelen [4] suggest to only diffuse particles carrying more circulation than a prescribed threshold. In their work, they set this threshold to the machine epsilon for single-precision floating-point arithmetic, i. e., round about $5.96 \cdot 10^{-8}$.

While choosing a threshold near machine accuracy does produce accurate results, this choice remains rather arbitrary. It is also not clear how big the

introduced error is. Luckily our analysis of the error may be extended to allow for the exclusion of particles from diffusion. Let \mathcal{I} be the set of particles that are not diffused and let $\tilde{\Delta}_h$ refer to the corresponding ‘reduced’ approximation of the Laplacian:

$$\tilde{\Delta}_h \omega(\mathbf{x}) := \sum_{i \notin \mathcal{I}} \sum_{j=1}^N \Gamma_i f_{ij} \delta(\mathbf{x} - \mathbf{x}_j). \quad (39)$$

Using the same techniques as above, we can then investigate the additional error introduced:

Theorem 4. *One has:*

$$\left\| (\Delta_h - \tilde{\Delta}_h) \omega \right\|_{W^{-k,q}} \leq 4(rh)^{-2} C_{\text{emb}} \|(\Gamma_i)_{i \in \mathcal{I}}\|_{l^1}.$$

PROOF. We have with Hölder’s inequality:

$$\begin{aligned} | \langle (\Delta_h - \tilde{\Delta}_h) \omega, \varphi \rangle | &= \left| \sum_{i \in \mathcal{I}} \sum_{j=1}^N \Gamma_i f_{ij} \varphi(\mathbf{x}_j) \right| \\ &\leq \|(\Gamma_i)_{i \in \mathcal{I}}\|_{l^1} \left\| \left(\sum_{j=1}^N f_{ij} \varphi(\mathbf{x}_j) \right)_{i \in \mathcal{I}} \right\|_{l^\infty}. \end{aligned} \quad (40)$$

Applying the triangle-inequality, Lemma 1 and the Sobolev embedding yields the result. \square

For the additional error to be of the same order as the error of the full scheme, we introduce a new user defined constant C_{diff} and require:

$$\|(\Gamma_i)_{i \in \mathcal{I}}\|_{l^1} \leq C_{\text{diff}} h^{n+2} \|(\Gamma_i)_i\|_{l^1}. \quad (41)$$

To minimise the number of diffused particles, we ignore those with the smallest amount of individual circulation, until this bound is reached. Using the same methods as above, it is easily verified that the reduced operator does conserve circulation and linear momentum, however, it does *not* conserve angular momentum.

3.6. Limitations of the Method

After having investigated consistency, stability, and conservation properties of the method we want to make some comments on its limitations. First, we

want to point out that unlike claimed by Shankar and van Dommelen [4] the vorticity redistribution method *does not* extend to arbitrary orders of accuracy. The stability proof relies on the fact that the stencils are non-negative. While other stable stencils might and probably do exist, we are not aware of any stability proof. As Seibold [7, 8] points out, any third or higher order method needs to fulfil the moment conditions for $|\alpha| = 4$. A simple linear combination of these equations yields:

$$\sum_{j \neq i} f_{ij} |\mathbf{r}_{ij}|^4 = 0, \quad (42)$$

which due to the non-negativity constraint can only be fulfilled for $f_{ij} \equiv 0$. The zero stencil, however, is inconsistent with the moment conditions for $|\alpha| = 2$. We may point out, however, that the method of particle strength exchange (PSE) similarly requires a positive kernel function for its stability proof, thereby equally limiting it to second order accuracy [1].

Secondly, we point out that the matrix F discontinuously depends on the particle positions: as they move around, they may enter and leave each other's neighbourhoods, allowing for jumps between zero and non-zero in the corresponding entries f_{ij} . In fact, in general, the solution to the moment equations is not even unique. It is thus hard to analyse the effect of higher-order time-stepping schemes on the method's accuracy.

4. Implementation

It has been claimed that the VRM is a slow algorithm, especially when compared to the PSE scheme, e.g., by Cottet and Koumoutsakos [1]. On the other hand, Schrader et al. [3] report that their DC-PSE method also takes up as much as 90% of total CPU time, and compare its computational speed with that of the VRM. We believe that the computational cost associated with the VRM has been greatly overestimated; mostly due to implementation issues. In this section we discuss some of these issues and illustrate a heuristic which can further speed up the method significantly. In our final implementation the

velocity computation took about three times longer than the evaluation of the discrete Laplacian.

4.1. Solution of the Moment Equations

Equation (10) is a classical ‘phase I problem’ of the Simplex algorithm for linear programming problems. When we use an insertion scheme such as the one described in section 4.2 this system is underdetermined, with a fixed, small number of rows $m = 5$ or $m = 9$, corresponding to the number of moment conditions, and a variable number of columns, corresponding to the size of the neighbourhood $\mathcal{N}_i \setminus \{i\}$.

The theory of simplex algorithms is too vast to be treated in detail here, such that we can only give a few key remarks and refer to the literature, e. g., Fletcher’s book [13], for further details. Assuming that the moment conditions do have a solution, phase I of the algorithm always returns one with m non-zero entries corresponding to a certain subset of particles in the neighbourhood. These non-zero entries are called basic variables. Setting the fractions f_{ij} for the remaining particles to zero, the solution can be obtained by solving an $m \times m$ linear system. The simplex algorithm is a systematic, iterative way of finding a valid set of basic variables. In every iteration of the algorithm an $m \times m$ system consisting of varying sets of columns of \mathbf{V}_i needs to be solved, typically by means of an LU-decomposition, which is of $\mathcal{O}(m^3)$ complexity [14].

The efficiency of the method thus crucially depends on the number of rows of \mathbf{V}_i , which should be kept as small as possible. Shankar and van Dommelen [4] use a different linear programming problem, aiming to minimise the maximum norm of the solution. By doing so, they solve a problem involving $4m$ rows, effectively making each iteration 64 times more expensive. One should thus keep the original formulation (10). Furthermore, optimising the solution with respect to some target value forces the algorithm to enter phase II, which further increases its cost without improving the method’s order of convergence. One might try to optimise the error constant by choosing an optimisation criterion that favours close particles. However, in regard of the later introduced heuristic of small

neighbourhoods in section 4.3, it is not immediately clear if this additional optimisation step is cheaper than choosing smaller values of h .

Note that the two possible values of m are very small and fixed. An efficient implementation should thus make use of this fact: all loops of the LU-decomposition can be unrolled, enabling compilers to perform aggressive optimisations. The LAPACK routines, on the other hand, were optimised for larger problems with dynamic, varying sizes [15].

There are several approaches to avoid a from-scratch computation of the LU-decomposition in every iteration of the method. Updating LU-decompositions instead of recomputing them, however, typically is only effective for larger values of m : the Fletcher–Matthews update, for example, is reported to be effective for $m > 10$ [16].

Note that the matrix V_i is fully populated and—as the number of neighbours is typically limited—of small to moderate size. On the other hand, most available implementations of the Simplex algorithm as well as a substantial part of the available literature focus on large-scale, sparse problems. In other words, they are optimised for the opposite case and thus cannot deliver good performance for our problem. Implementing an efficient, dense simplex method is essential for the overall performance of the VRM. As this task is not straight forward, some authors, e. g., Lakkis and Ghoniem [17], prefer to solve the non-negative least-squares problem instead:

$$\min_{f_i \geq 0} |V_i f_i - \mathbf{b}_i|^2, \quad (43)$$

where $|\cdot|$ refers to the Euclidean norm. This problem can be solved using the algorithm due to Lawson and Hanson [18], which solves an *unconstrained* least-squares problem in each iteration. However, the size of this unconstrained problem varies in every iteration, making it harder to unroll loops a priori. Additionally, these problems are typically solved using QR- or LQ-decompositions, which are more expensive than the LU-decomposition. We therefore do not further pursue this approach.

4.2. Insertion of New Particles

In order to ensure that non-negative stencils exist, particles need to have sufficiently many neighbours which also need to fulfil certain geometric conditions. Seibold [7, 8] gives the exact conditions for the first order case $n = 1$ as well as the following sufficient condition: seen from the centre of the neighbourhood, the angle between two adjacent particles may be no more than 45° . Assuming a given maximum hole-size in the particle cloud, he also gives a sufficient upper bound Rh for the neighbourhood size. These conditions could in principle be implemented in a VRM scheme, resulting in a strong guarantee that positive stencils always exist.

However, as he points out, these conditions are often too strict. We thus pursue a different approach. Instead of directly checking the angles between each pair of adjacent particles, we subdivide the neighbourhood into eight segments of 45° each, as illustrated in figure 1. In order to avoid wasting computational resources, we do not want to insert new particles that would violate the lower bound in (5) for any other particle. However, we also want to avoid small values of r , to prevent the time-step constraint (27) from becoming too strict. As a compromise we choose $r = 1/2$ and $R = 2$ and apply the following insertion strategy: if any neighbourhood segment contains no particles, a new particle is inserted on the segment's centre line at radial position $1.5h$. As illustrated in figure 1, this ensures that the newly inserted particle does not violate any other particle's lower bound on its neighbourhood.

This insertion strategy ensures that particles are at most spaced $2h$ apart. According to theorem 6.11 of Seibold's thesis, choosing the upper bound of the neighbourhood size as $R \geq 5.23$ then guarantees the existence of positive stencils. However, in our numerical experiments, such a large choice was not necessary and all computations worked well with $R = 2$. Experiments conducted with a slightly rotated reference frame indicated that the results of this strategy do not significantly depend on the coordinate system used.

Unlike claimed by Cottet and Koumoutsakos [1], insertion of empty particles is different from remeshing: it leaves the vorticity field (1) unchanged, thereby

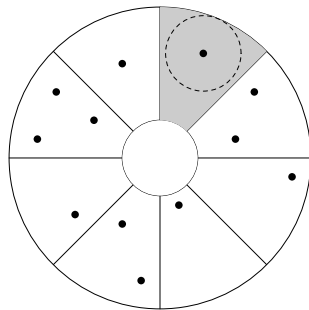


Figure 1: Illustration of a particle neighbourhood and the insertion strategy. Each of the eight segments except for the shaded one contained at least one particle. In the shaded segment a new particle is inserted on the centre line at radial position $1.5h$. No particle can be closer than $0.5h$ to the newly inserted particle: the circle of that radius is indicated using a dashed line and is completely included in the previously empty segment.

introducing no error and it does not rearrange existing particles. For this reason the VRM is a truly mesh-free method.

4.3. *Small Neighbourhoods*

As pointed out in section 4.1, the simplex method systematically determines a subset of particles leading to a non-negative solution of the moment equations. One can consequently lower iteration counts by reducing the number of particles in the neighbourhood. In most cases a non-negative solution exists if there is just one particle in every 45° -segment of the neighbourhood. This leads us to the following approach: for every particle neighbourhood, choose the closest particle of each segment. We call the resulting subset the *small neighbourhood*. We then apply the simplex method to this small neighbourhood. By choosing the segments' closest particles, we aim to locally reduce R , thereby minimising the error constant. Only if no non-negative solution was found, we retry with the complete neighbourhood. In our numerical examples, depending on h , this only happened in a negligible (less than a hundred) number of cases.

This approach has the advantage that *all* matrices and vectors involved in the simplex algorithm can be statically allocated, avoiding the overhead of dynamic memory allocation and further enabling the compiler to unroll more

loops. In our experiments in section 5.2, the use of these small neighbourhoods instead of the complete ones lead to a threefold speed-up.

Note that after the assembly of the Vandermonde matrices V_i , this approach leads to a set of completely decoupled, small problems of fixed size. We thus have an *embarrassingly parallel* problem, making it ideally suited for computations on many-core processors, such as GPUs or the Intel Xeon Phi.

5. Numerical Experiments

As Shankar and van Dommelen point out in their work [4], the Lamb–Oseen flow is an ideal test-case for vortex particle methods: its initial condition is a single Dirac delta distribution:

$$\omega(0, \mathbf{x}) = \Gamma \delta(\mathbf{x}), \quad (44)$$

and can thus be exactly represented in a vortex particle method. The analytic solution is infinitely smooth and valid for the heat-equation (18) as well as the vorticity-transport equation (2):

$$\omega(t, \mathbf{x}) = \frac{\Gamma}{4\pi\nu t} e^{-\frac{|\mathbf{x}|^2}{4\nu t}} \quad (t > 0). \quad (45)$$

The corresponding velocity field is given by:

$$\mathbf{u}(t, \mathbf{x}) = \frac{\Gamma}{2\pi|\mathbf{x}|} \left(1 - \exp\left(-\frac{|\mathbf{x}|^2}{4\nu t}\right) \right) \hat{\varphi}, \quad (46)$$

where $\hat{\varphi}$ refers to the unit vector in circumferential direction at position \mathbf{x} . In the following, we will describe several numerical experiments carried out on this flow. Mimicking Shankar and van Dommelen’s case of $\text{Re} = 50$, we chose $n = 1$, $\Gamma = 2\pi$, $C_{\text{diff}} = 1$, $\nu = 1/50$. We choose higher resolutions, however, and stop time-integration at $t = 1$.

5.1. Convergence with respect to h

We consider the cases with and without convection, corresponding to the Navier–Stokes equation and the heat equation, respectively. In the case of the

heat equation, we use Euler’s method to advance the solution in time and choose a fixed time step:

$$\Delta t = \frac{1}{8} \frac{(rh)^2}{4\nu}. \quad (47)$$

As mentioned previously, in vortex methods it is customary to replace the singular Biot–Savart kernel \mathbf{K} with a regularised one \mathbf{K}_ε . We use the following second order kernel obtained after Gaussian smoothing:

$$\mathbf{K}_\varepsilon(\mathbf{x}) = \frac{(-y, x)^\top}{2\pi|\mathbf{x}|^2} \left(1 - \exp\left(-\left|\frac{\mathbf{x}}{\varepsilon}\right|^2\right) \right), \quad \mathbf{x} = (x, y)^\top.$$

Our particle insertion strategy guarantees that particles are at most spaced $2h$ apart. To ensure sufficient overlap we choose $\varepsilon = 3h$. A fast multipole method (FMM) similar to that of Dehnen [19] of order $p = 16$ and multipole acceptance criterion $\theta \leq 0.8$ is used to speed up the velocity computation.

Practical experience has shown, that higher order time-stepping methods are required to maintain linear and angular momentum in the case of enabled convection. Like Shankar and van Dommelen, we choose the classical Runge–Kutta method (RK4) in this case. In order to resolve particle movement accurately, the time-step is adaptively chosen as the minimum of (47) and the following CFL-type condition:

$$\Delta t \leq \frac{1}{8} \min_{i=1, \dots, N} \frac{h}{|\mathbf{u}_i|}. \quad (48)$$

We want to stress that this second bound is not required to ensure stability: experiments without this restriction showed no instabilities and gave reasonable results, however, the errors in linear and angular momentum were larger.

As it is difficult to compute Sobolev-norm $\|\cdot\|_{W^{-k,q}}$ explicitly, we try to approximate the L^2 -error of the corresponding velocity. As the system contains infinite energy, we need to limit the area of integration. We chose $A = [-1.5, 1.5]^2$, as all particles were contained within this region. By means of numerical quadrature we then evaluate:

$$e_{\mathbf{u}} = \frac{\|\mathbf{u} - \mathbf{u}_h\|_{L^2(A)}}{\|\mathbf{u}\|_{L^2(A)}}, \quad (49)$$

where \mathbf{u}_h stands for the velocity field which is obtained from the particle approximation for a chosen value of h using the smoothed kernel \mathbf{K}_ε .

Figure 2 shows the observed error estimates for various values of h . Even though the expected convergence rate was $n = 1$, we actually observe second order convergence behaviour. This is similar to the observations by Seibold, who explains this using a symmetry argument: the classical five-point finite-difference stencil achieves second order accuracy due to the symmetry of the particle locations. However, the insertion strategy and the definition of the particle neighbourhoods preclude extreme cases of asymmetry, which might result in the observed second order convergence. Seibold, however, does not exclude particles according to equation (41). It thus comes as a surprise that even the reduced operator exhibits this behaviour. As both curves form a nearly straight line and essentially coincide, we suspect that the smoothing error dominates for this choice of parameters.

Figure 3 shows the number of particles in the final time-step of the computation. It increases approximately as $\mathcal{O}(h^{-2})$, as one would expect in a grid-based computation. This again is surprising, as bound (41) gets stricter for decreasing h . Due to the convection in the Navier–Stokes case, more particles need to be inserted as they move around. In our simulation, this caused an increase in the number of particles of a nearly constant factor 1.6.

As shown in section 3.5, the reduced operator conserves circulation and linear momentum exactly. In the case of the heat equation this remains the case when a time-stepping scheme is applied: the error in I_0 and \mathbf{I}_1 was of the order of the machine accuracy. For the Navier–Stokes equation this is only true for the circulation. For all choices of h the error in linear momentum varied between $\mathcal{O}(10^{-6})$ and $\mathcal{O}(10^{-7})$. We believe this to be a result of the limited accuracy of the FMM code that was used for the velocity computation and the error introduced by the Runge–Kutta method. Figure 4 shows the error in angular momentum I_2 . The values for the heat equation decrease at a rate of $\mathcal{O}(h^3)$, similar to the bound (41). In the convective case the error decays somewhat faster, in a less clear-cut manner. We believe this to be a result of the increased number of particles. We thus conclude that for the chosen values of h , the error

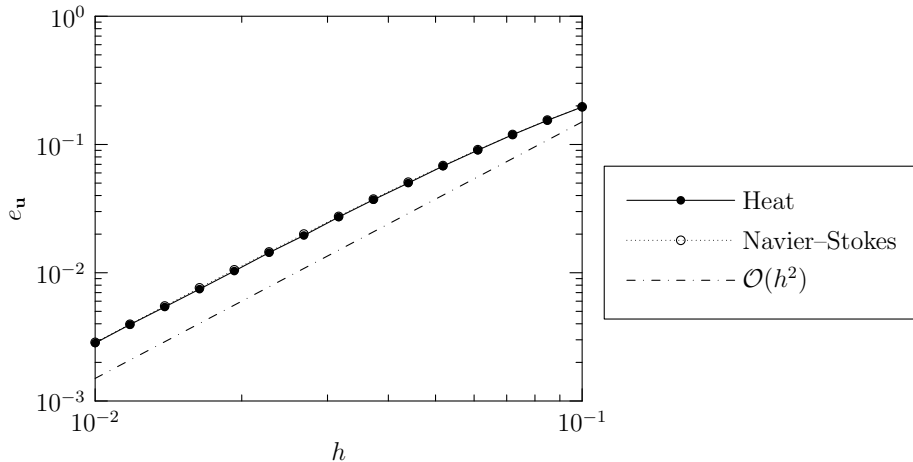


Figure 2: Error estimates for the heat and Navier–Stokes equations for varying values of h at $t = 1$. Their values essentially coincide and exhibit an $\mathcal{O}(h^2)$ convergence behaviour.

in angular momentum induced by using the reduced operator (39) dominates that of the FMM and the time-stepping scheme.

Figure 5 shows the velocity at the particle locations for $h = 0.04$ at $t = 1$ with enabled convection. Despite the asymmetry in the particle locations caused by the convection, one can see that the velocity field remains quite symmetric. The reduced operator prevents the creation of particles that would carry insignificant amount of circulation. For this reason, the particle cloud takes the shape of a circle around the origin: vorticity decays exponentially with the distance to the origin. At $\varepsilon = 3h = 0.12$ the resolution is not high enough to accurately represent steep velocity gradient at the centre of the flow. However, due to the good conservation properties, we obtain a qualitatively good solution already at this under-resolved computation.

5.2. Computational Speed

In order to assess the speed of the method, we measured the time needed to evaluate the velocity and the Laplacian for $h = 0.01$. For the Laplacian, we compared the performance of two codes: the first code uses LAPACK to decompose the arising linear systems in each simplex iteration and takes the

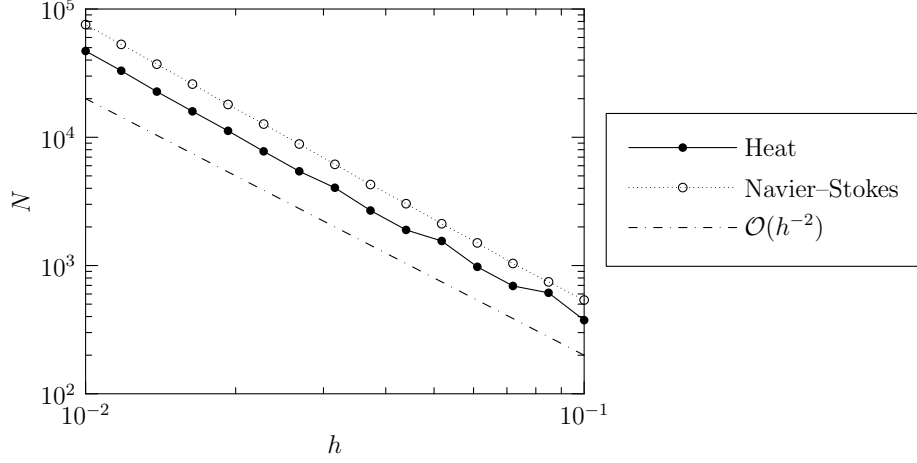


Figure 3: The number of particles in the final step of the computation for the heat and Navier–Stokes equations. The curves show a particle growth that scales as $\mathcal{O}(h^{-2})$, despite the fact that equation (41) is getting stricter for decreasing mesh-sizes. The ratio between the two curves’ values remains approximately fixed at around 1.6.

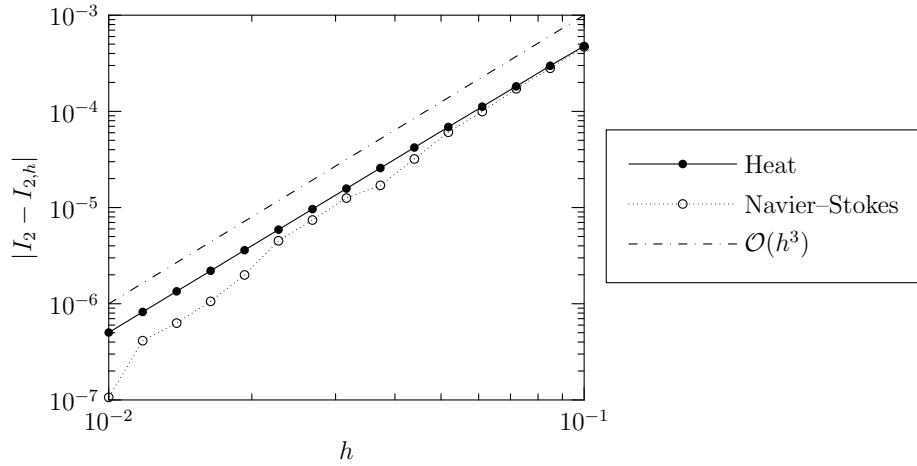


Figure 4: Error in angular momentum at the final time-step for the heat and Navier–Stokes equations. The error decays at a rate of $\mathcal{O}(h^3)$, the same exponent as in condition (41). In case of the Navier–Stokes equations, the error decreases even faster, in a less clear-cut manner.

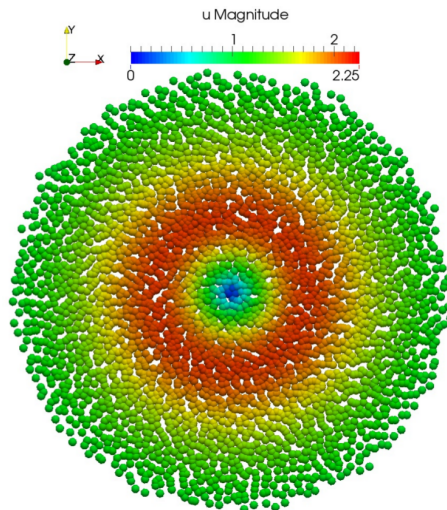


Figure 5: Plot of the smoothed velocity at the particle locations for $h = 0.04$ at $t = 1$. Despite the asymmetric particle distribution, caused by the convection, the velocity field remains very symmetric. The particle cloud takes the shape of a circle. Even in this under-resolved case, the method yields qualitatively good results.

complete particle neighbourhood into account. The second code uses small neighbourhoods as described in section 4.3 and an implementation using completely unrolled loops in the LU-decomposition. The code was parallelised using OpenMP, where task-based parallelism was used for the FMM.

Figure 6 shows the required time for each computation depending on the number of particles involved. One can see that all computations scale linearly with N , however, with different constant factors. The code using small neighbourhoods performs about three times faster than the corresponding code using the complete ones. This clearly highlights the benefit of trying small neighbourhoods first. It also performs about three times as fast as the corresponding FMM code. Further measurements showed that, in the case of small neighbourhoods, only about one third of the time was used for the actual simplex solver, while the remaining time was spent finding neighbourhoods and inserting new particles. A hash-based algorithm was used for this, causing the resulting curve to be jagged due to caching effects.

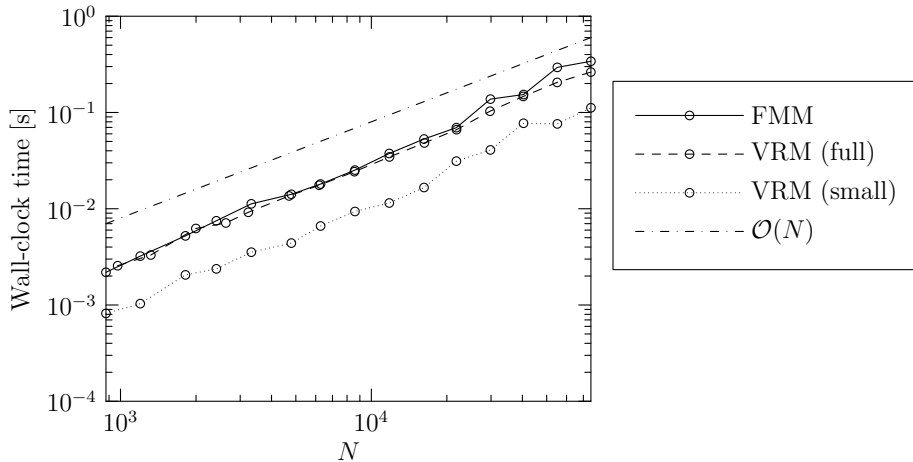


Figure 6: Required CPU time for the VRM with the full and small neighbourhoods in comparison to the FMM. The computations were performed on an Intel Xeon E5-1650v3, a six-core processor running at 3.5 GHz. The line corresponding to the FMM is jagged due to the task-based parallelism used in the implementation. The VRM computation can be greatly accelerated using small neighbourhoods, it is then about three times faster than the corresponding velocity computation.

Note that these numbers cannot be directly compared to those reported by Shankar and van Dommelen: they compare a single VRM computation to that of a convective step performed using the Runge–Kutta method, i. e., involving four velocity computations. In this setting, their VRM computation takes about 25% longer than the convective step, i. e., five times longer than a single velocity evaluation. In comparison to the respective FMM codes, our VRM computation thus is about 15 times faster.

6. Conclusion and Outlook

6.1. Conclusion

We have introduced a splitting-free variant of the vorticity redistribution method (VRM). Using the new concept of small-neighbourhoods, its speed compared to the original method can be greatly accelerated and typically is below that of the corresponding velocity computation. Equation (41) allows us to efficiently and consistently reduce the number of diffused particles. We have

illustrated that the method can be implemented efficiently and that previous claims on the slow speed of the VRM are probably due to implementation issues. The large number of small, independent, fixed-size problems involved makes it an ideal candidate for parallelisation on coprocessors such as GPUs or the Intel Xeon Phi. We conclude this text with a few possible extensions on the method.

6.2. Outlook

In light of the quadratic time-step bound (27), an interesting topic for future research might be the application of implicit time-stepping schemes in periodic flows. As the convective part of the equations is non-stiff, this seems to be an ideal use-case for IMEX multistep schemes [21]. After having convected the particles, F could then be readily assembled, leading to a linear system. As Seibold discusses in his work [9], due to the positivity and sparsity of the stencils, such systems can effectively be solved using algebraic multigrid methods.

The definition of a particle's neighbourhood in equation (5) excludes particles that are too close to that particle. In order to save computational resources, it may thus be desirable to remove particles in areas where they get too close to one another. Instead of approximating the Laplacian as described in this article, one can apply the same methodology to approximate the identity operator using a particle's neighbours. This way, a particle can be redistributed to its neighbours and subsequently be removed. Lakkis and Ghoniem [17] successfully applied a similar procedure and reported a significant reduction in the number of particles.

Finally, we would like to conclude this text by thanking the editor and reviewers for their comments which helped improving the quality of this article. This work was financially supported by the Keio Leading-edge Laboratory of Science and Technology (KLL). The first author also receives the MEXT scholarship of the Japanese Ministry of Education.

References

References

- [1] G.-H. Cottet, P. D. Koumoutsakos, *Vortex Methods*, Cambridge University Press, 2000.

- [2] L. F. Rossi, Resurrecting core spreading vortex methods: A new scheme that is both deterministic and convergent, *SIAM Journal on Scientific Computing* 17 (2) (1996) 370–397.
- [3] B. Schrader, S. Reboux, I. F. Sbalzarini, Discretization correction of general integral PSE Operators for particle methods, *Journal of Computational Physics* 229 (11) (2010) 4159–4182.
- [4] S. Shankar, L. van Dommelen, A new diffusion procedure for vortex methods, *Journal of Computational Physics* 127 (1) (1996) 88–109.
- [5] J. T. Beale, A. J. Majda, Rates of convergence for viscous splitting of the Navier–Stokes equations, *Mathematics of Computation* 37 (156) (1981) 243–259.
- [6] C. Anderson, C. Greengard, On vortex methods, *SIAM Journal on Numerical Analysis* 22 (3) (1985) 413–440.
- [7] B. Seibold, M-matrices in meshless finite difference methods, Ph.D. thesis, Technische Universität Kaiserslautern, Fachbereich Mathematik (September 2006).
- [8] B. Seibold, Minimal positive stencils in meshfree finite difference methods for the poisson equation, *Computer Methods in Applied Mechanics and Engineering* 198 (3–4) (2008) 592–601.
- [9] B. Seibold, Performance of algebraic multigrid methods for non-symmetric matrices arising in particle methods, *Numerical Linear Algebra with Applications* 17 (2–3) (2010) 433–451.
- [10] S. Gottlieb, C.-W. Shu, E. Tadmor, Strong stability-preserving high-order time discretization methods, *SIAM Review* 43 (1) (2001) 89–112.
- [11] A. J. Majda, A. L. Bertozzi, *Vorticity and Incompressible Flow*, Cambridge University Press, 2001.

- [12] T. Tao, Conserved quantities for the Euler equations, Personal Blog Entry (February 2014).
URL <https://terrytao.wordpress.com>
- [13] R. Fletcher, Practical Methods of Optimization, 2nd Edition, Wiley, 2000.
- [14] G. H. Golub, C. F. Van Loan, Matrix Computations, 4th Edition, John Hopkins University Press, 2013.
- [15] E. Anderson et al., LAPACK User's Guide, Society for Industrial and Applied Mathematics, 1999.
- [16] R. Fletcher, S. P. J. Matthews, Stable modification of explicit lu factors for simplex updates, *Mathematical Programming* 30 (3) (1984) 267–284.
- [17] I. Lakkis, A. Ghoniem, A high resolution spatially adaptive vortex method for separating flows. part i: Two-dimensional domains, *Journal of Computational Physics* 228 (2) (2009) 491–515.
- [18] C. L. Lawson, R. J. Hanson, Solving Least Squares Problems, Classics in Applied Mathematics, Society for Industrial and Applied Mathematics, 1995.
- [19] W. Dehnen, A hierarchical $o(n)$ force calculation algorithm, *Journal of Computational Physics* 179 (1) (2002) 27–42.
- [20] P. Ploumhans, G. S. Winckelmans, J. K. Salmon, A. Leonard, M. S. Warren, Vortex methods for three-dimensional bluff body flows: Application to the sphere at $re=300, 500$ and 1000 , *Journal of Computational Physics* 178 (2) (2002) 427–463.
- [21] U. M. Ascher, S. J. Ruuth, B. T. Wetton, Implicit-explicit methods for time-dependent partial differential equations, *SIAM Journal on Numerical Analysis* 32 (3) (1993) 797–823.